Lecture 9: Triggering Transition: Towards Minimal Seeds

Rich Kerswell

Notes by Andrew Crosby, Keiji Kimura

30 June 2011

1 Introduction

In the previous lecture we discussed the edge and tracking it *forward* in time to a relative attractor - the edge state. This always seems to be on an energy plateau compared with other points and it is natural to ask what is the lowest energy attained by the edge. The initial condition corresponding to this point - the *minimal seed* - infinitesimally disturbed represents the easiest way (energetically) to trigger turbulence. In this lecture, we discuss a method of finding the minimal seed which, in some sense, manages to integrate *backwards* in time along the edge.

Some evidence that there is a disparity in energies on the edge was supplied recently by Viswanath and Cvitanović [13] who looked at shooting for the edge state in a short pipe of length πD (D is the pipe diameter). They took a combination of only three flow fields as an initial condition and searched for the lowest initial energy for which the ensuing flow would approach a particular travelling wave solution some time later. This travelling wave was chosen as the target since it is known to be embedded in the chaotic edge state in a $5D$ pipe [7]. They chose one of the initial flow fields as the travelling wave solution itself and the other two to be its two unstable eigenmodes, and found that the maximum growth ratio of the energy was $O(10^4)$ (see also [4]). Thus some regions of the edge have a much smaller energy level than the attracting plateau where the edge state resides. This suggests a strategy to identify the minimal seed which involves looking for the initial condition which experiences the largest energy growth. A brute force search over all possible initial conditions is not feasible but a variational approach is.

We define the growth of the energy at time T by the gain

$$G(T) := \max_{\mathbf{u}_0(\mathbf{x}),\ \nabla\cdot\mathbf{u}_0=0} \frac{\left\langle \frac{1}{2}|\mathbf{u}(\mathbf{x},T)|^2 \right\rangle}{\left\langle \frac{1}{2}|\mathbf{u}_0(\mathbf{x})|^2 \right\rangle}, \tag{1}$$

where $\mathbf{u}_0(\mathbf{x}) = \mathbf{u}(\mathbf{x}, t=0)$ and $\langle\cdot\rangle$ means the volume integration $\int \cdot\, dV$. It is this function $G(T)$ that we want to maximise to find the minimal seed. We briefly discuss the matrix-based and a matrix-free variational methods to find the minimal seed of the linearised

Navier-Stokes equations. Then we extend the matrix-free approach to investigate the fully nonlinear transient energy growth problem [8],[9].

2 Linear transient energy growth (non-modal analysis)

The non-dimensionalized linearized Navier-Stokes equation around the laminar flow $\mathbf{u}_{\text{lam}}$ is

$$\frac{\partial \mathbf{u}}{\partial t} + (\mathbf{u}_{\text{lam}} \cdot \nabla)\mathbf{u} + (\mathbf{u} \cdot \nabla)\mathbf{u}_{\text{lam}} + \nabla p = \frac{1}{Re}\nabla^2 \mathbf{u}, \tag{2}$$

where $\mathbf{u}$ is the perturbation of the laminar flow $\mathbf{u}_{lam}$ and Re is the Reynolds number. As normal we assume that the fluid is incompressible, $\nabla \cdot \mathbf{u} = 0$.

2.1 Matrix-based method

We can rewrite the linearized Navier-Stokes equation (2) in the form

$$\frac{\partial \mathbf{u}}{\partial t} = L\mathbf{u}, \tag{3}$$

where L is a linear operator, which has eigenvalues λ_j and eigenfunctions $\mathbf{q}_j$. Assuming that the set $\mathbf{q}_j$ is complete (but not necessarily orthogonal unless L is normal), then

$$\mathbf{u}_0(\mathbf{x}) = \sum_{j=1}^{\infty} a_j(0)\mathbf{q}_j(\mathbf{x}) \quad \Rightarrow \quad \mathbf{u}(\mathbf{x}, t) = \sum_{j=1}^{\infty} a_j(t)\mathbf{q}_j(\mathbf{x}) \tag{4}$$

where $a_j(t) := a_j(0)\exp(\lambda_j t)$. Then

$$G(T; Re) = \max_{\mathbf{a(0)}} \frac{\langle\, \mathbf{u}^* \,.\, \mathbf{u} \,\rangle}{\langle\, \mathbf{u}_0^* \,.\, \mathbf{u}_0 \,\rangle} = \max_{\mathbf{a(0)}} \frac{\sum_i \sum_j a_i^*(T) a_j(T) \langle\, \mathbf{q}_i^* . \mathbf{q}_j \,\rangle}{\sum_i \sum_j a_i^*(0) a_j(0) \langle\, \mathbf{q}_i^* . \mathbf{q}_j \,\rangle}. \tag{5}$$

Truncating at some large but finite N (so things become finite-dimensional yet insensitive to the exact value of N) then $M_{ij} := \langle\, \mathbf{q}_i^* . \mathbf{q}_j \,\rangle$ is a Hermitian $n \times n$ matrix which can be reduced to another matrix F such that $F^*F = M$, then

$$G(T; Re) = \max_{\mathbf{a(0)}} \frac{[F\mathbf{a}(T)]^* . F\mathbf{a}(T)}{[F\mathbf{a}(0)]^* . F\mathbf{a}(0)} = \max_{\mathbf{a(0)}} \frac{[Fe^{\Lambda T}\mathbf{a}(0)]^* . Fe^{\Lambda T}\mathbf{a}(0)}{[F\mathbf{a}(0)]^* . F\mathbf{a}(0)} = ||Fe^{\Lambda T}F^{-1}||_2^2 \tag{6}$$

where $e^{\Lambda T} = \text{diag}(e^{\lambda_1 T}, e^{\lambda_2 T}, \ldots, e^{\lambda_N T})$ [11]. This can handled by standard Singular Value Decomposition (SVD) software to give the largest singular value. If L is normal, M and F are diagonal and

$$G(T; Re) = ||e^{\Lambda T}||_2^2 = \max_j \left| e^{\lambda_j T} \right|^2 = \max_j e^{2\Re e(\lambda_j)T} \tag{7}$$

so there can be no transient growth when L is linearly stable i.e. $\Re e(\lambda_j) \leq 0$ for all j.

This method is straightforward but only really computationally feasible for one-dimensional, or possibly two-dimensional problems because the size of the matrices becomes unwieldy and then unmanageable for three-dimensional problems. A better approach is the matrix-free method which, although incurring more start-up costs (e.g. building a time stepping algorithm), is extendable to include nonlinearity.

2.2 Matrix-free method – Variational method

In this section, we consider the use of a matrix-free variational method for finding the energy growth which involves time-stepping the linearised Navier-Stokes equations. Since the problem is linear, the initial energy can be rescaled to 1 and we consider the Lagrangian

$$\begin{aligned} G = G(\mathbf{u}, p, \lambda, \boldsymbol{\nu}, \pi; T) &= \left\langle \frac{1}{2}|\mathbf{u}(\mathbf{x}, T)|^2 \right\rangle + \lambda \left\{ \left\langle \frac{1}{2}|\mathbf{u}(\mathbf{x}, 0)|^2 \right\rangle - 1 \right\} \\ &+ \int_0^T \left\langle \boldsymbol{\nu}(\mathbf{x}, t) \cdot \left\{ \frac{\partial \mathbf{u}}{\partial t} + (\mathbf{u}_{\text{lam}} \cdot \nabla)\mathbf{u} + (\mathbf{u} \cdot \nabla)\mathbf{u}_{\text{lam}} + \nabla p - \frac{1}{Re}\nabla^2 \mathbf{u} \right\} \right\rangle dt \\ &+ \int_0^T \langle \pi(\mathbf{x}, t) \nabla \cdot \mathbf{u} \rangle \, dt \end{aligned} \tag{8}$$

where λ, $\boldsymbol{\nu}$ and π are Lagrangian multipliers imposing the constraints that the initial energy is fixed, that the linearized Navier-Stokes equation (2) holds over $t \in [0, T]$ and the flow is incompressible (their corresponding Euler-Lagrange equations are respectively:

$$\left\langle \frac{1}{2}|\mathbf{u}(\mathbf{x}, 0)|^2 \right\rangle = 1, \tag{9}$$

$$\frac{\partial \mathbf{u}}{\partial t} + (\mathbf{u}_{\text{lam}} \cdot \nabla)\mathbf{u} + (\mathbf{u} \cdot \nabla)\mathbf{u}_{\text{lam}} + \nabla p - \frac{1}{Re}\nabla^2 \mathbf{u} = 0, \tag{10}$$

$$\nabla \cdot \mathbf{u} = 0.) \tag{11}$$

The Euler-Lagrange equation for the pressure p is

$$\begin{aligned} 0 &= \int_0^T \left\langle \frac{\delta G}{\delta p} \delta p \right\rangle dt = \int_0^T \langle (\boldsymbol{\nu} \cdot \nabla)\delta p \rangle \, dt \\ &= \int_0^T \langle \nabla \cdot (\boldsymbol{\nu} \delta p) \rangle \, dt - \int_0^T \langle \delta p (\nabla \cdot \boldsymbol{\nu}) \rangle \, dt. \end{aligned} \tag{12}$$

which to vanish means

$$\boldsymbol{\nu} = \mathbf{0} \ \text{ at boundary}, \tag{13}$$

$$\nabla \cdot \boldsymbol{\nu} = 0. \tag{14}$$

Finally, considering variations in $\mathbf{u}$ (with the condition that $\delta\mathbf{u} = \mathbf{0}$ on the boundary):

$$\begin{aligned} \int_0^T \left\langle \frac{\delta G}{\delta \mathbf{u}} \cdot \delta \mathbf{u} \right\rangle &= \langle \mathbf{u}(\mathbf{x}, T) \cdot \delta \mathbf{u}(\mathbf{x}, T) \rangle + \lambda \langle \mathbf{u}(\mathbf{x}, 0) \cdot \delta \mathbf{u}(\mathbf{x}, 0) \rangle \\ &+ \int_0^T \left\langle \boldsymbol{\nu} \cdot \left\{ \frac{\partial \delta \mathbf{u}}{\partial t} + (\mathbf{u}_{\text{lam}} \cdot \nabla)\delta\mathbf{u} + (\delta\mathbf{u} \cdot \nabla)\mathbf{u}_{\text{lam}} - \frac{1}{Re}\nabla^2 \delta\mathbf{u} \right\} \right\rangle dt \\ &+ \int_0^T \langle \pi \nabla \cdot \delta \mathbf{u} \rangle \, dt. \end{aligned} \tag{15}$$

The first term in the second line of the above equation can be reexpressed as

$$\begin{aligned} \int_0^T \left\langle \boldsymbol{\nu} \cdot \frac{\partial \delta \mathbf{u}}{\partial t} \right\rangle dt &= \int_0^T \left\langle \frac{\partial}{\partial t}(\delta \mathbf{u} \cdot \boldsymbol{\nu}) \right\rangle dt - \int_0^T \left\langle \delta \mathbf{u} \cdot \frac{\partial \boldsymbol{\nu}}{\partial t} \right\rangle dt \\ &= \langle \delta \mathbf{u}(\mathbf{x}, T) \cdot \boldsymbol{\nu}(\mathbf{x}, T) - \delta \mathbf{u}(\mathbf{x}, 0) \cdot \boldsymbol{\nu}(\mathbf{x}, 0) \rangle - \int_0^T \left\langle \delta \mathbf{u} \cdot \frac{\partial \boldsymbol{\nu}}{\partial t} \right\rangle dt, \end{aligned} \tag{16}$$

the second term as

$$\begin{aligned}\langle \boldsymbol{\nu} \cdot \{(\mathbf{u}_{\rm lam} \cdot \nabla)\delta\mathbf{u}\}\rangle &= \langle \nabla \cdot ((\boldsymbol{\nu} \cdot \delta\mathbf{u})\mathbf{u}_{\rm lam}) - \delta\mathbf{u} \cdot \{(\mathbf{u}_{\rm lam} \cdot \nabla)\boldsymbol{\nu}\}\rangle \\ &= -\langle \delta\mathbf{u} \cdot \{(\mathbf{u}_{\rm lam} \cdot \nabla)\boldsymbol{\nu}\}\rangle\,, \end{aligned} \tag{17}$$

the third term as

$$\langle \boldsymbol{\nu} \cdot \{(\delta\mathbf{u} \cdot \nabla)\mathbf{u}_{\rm lam}\}\rangle = \left\langle \delta\mathbf{u} \cdot \left\{\boldsymbol{\nu} \cdot (\nabla\mathbf{u}_{\rm lam})^{\rm T}\right\}\right\rangle (= \langle \delta u_i\ \nu_j\ \partial_i u_{{\rm lam},j}\rangle). \tag{18}$$

and the fourth term as

$$\left\langle \boldsymbol{\nu} \cdot \left(-\frac{1}{Re}\nabla^2\delta\mathbf{u}\right)\right\rangle = -\left\langle \frac{1}{Re}\delta\mathbf{u} \cdot \nabla^2\boldsymbol{\nu}\right\rangle, \tag{19}$$

and finally the last term as

$$\begin{aligned}\langle \pi\nabla \cdot \delta\mathbf{u}\rangle &= \langle \nabla \cdot \pi\delta\mathbf{u}\rangle - \langle \delta\mathbf{u} \cdot \nabla\pi\rangle \\ &= -\langle \delta\mathbf{u} \cdot \nabla\pi\rangle\,. \end{aligned} \tag{20}$$

Combining all these gives

$$\begin{aligned}\int_0^T \left\langle \frac{\delta G}{\delta\mathbf{u}} \cdot \delta\mathbf{u}\right\rangle dt &= \langle \delta\mathbf{u}(\mathbf{x},T) \cdot \{\mathbf{u}(\mathbf{x},T) + \boldsymbol{\nu}(\mathbf{x},T)\}\rangle \\ &\quad + \langle \delta\mathbf{u}(\mathbf{x},0) \cdot \{\lambda\mathbf{u}(\mathbf{x},0) - \boldsymbol{\nu}(\mathbf{x},0)\}\rangle \\ &\quad + \int_0^T \left\langle \delta\mathbf{u} \cdot \left\{-\frac{\partial\boldsymbol{\nu}}{\partial t} - (\mathbf{u}_{\rm lam} \cdot \nabla)\boldsymbol{\nu} + \boldsymbol{\nu} \cdot (\nabla\mathbf{u}_{\rm lam})^{\rm T} - \nabla\pi - \frac{1}{Re}\nabla^2\boldsymbol{\nu}\right\}\right\rangle dt. \end{aligned} \tag{21}$$

For this to vanish for all allowed $\delta\mathbf{u}(\mathbf{x},T)$, $\delta\mathbf{u}(\mathbf{x},0)$ and $\delta\mathbf{u}$ means

$$\frac{\delta G}{\delta\mathbf{u}(\mathbf{x},T)} = 0 \quad \Rightarrow \quad \mathbf{u}(\mathbf{x},T) + \boldsymbol{\nu}(\mathbf{x},T) = \mathbf{0} \tag{22}$$

$$\frac{\delta G}{\delta\mathbf{u}(\mathbf{x},0)} = 0 \quad \Rightarrow \quad \lambda\mathbf{u}(\mathbf{x},0) - \boldsymbol{\nu}(\mathbf{x},0) = \mathbf{0} \tag{23}$$

$$\frac{\delta G}{\delta\mathbf{u}} = 0 \quad \Rightarrow \quad \frac{\partial\boldsymbol{\nu}}{\partial t} + (\mathbf{u}_{\rm lam} \cdot \nabla)\boldsymbol{\nu} - \boldsymbol{\nu} \cdot (\nabla\mathbf{u}_{\rm lam})^{\rm T} + \nabla\pi + \frac{1}{Re}\nabla^2\boldsymbol{\nu} = \mathbf{0}. \tag{24}$$

The last equation is the 'dual (or adjoint) linearized Navier-Stokes equation'. This equation can only be integrated backwards in time because of the negative diffusion term. Figure 1 shows a diagram of a numerical method for iteratively solving these variational equations in order to construct the initial condition with maximum growth (e.g. [5]). The algorithm has the following steps.

Step.0 Choose an initial condition of the iterative method $\mathbf{u}^{(0)}(\mathbf{x},0)$ such that

$$\left\langle \frac{1}{2}\left\{\mathbf{u}^{(0)}(\mathbf{x},0)\right\}^2\right\rangle = 1. \tag{25}$$

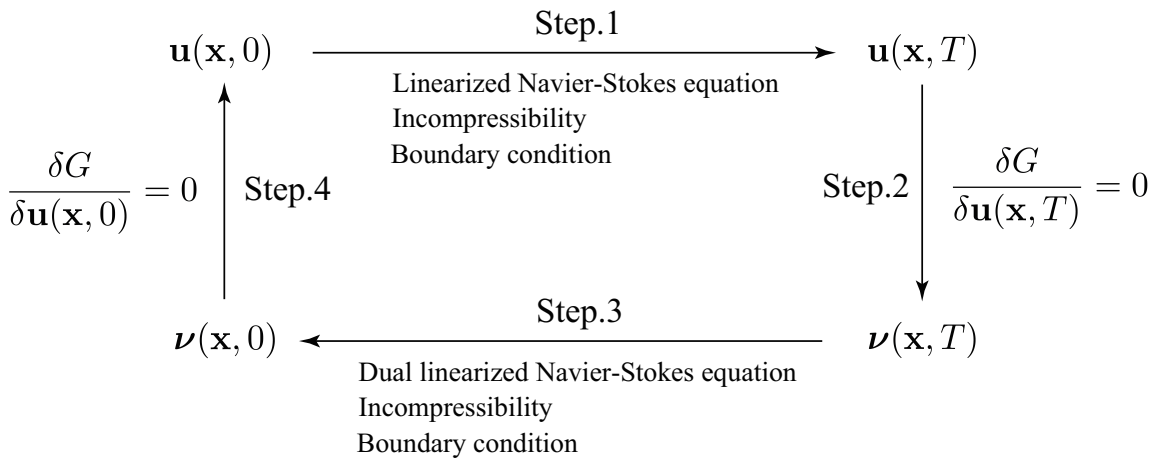

Figure 1: Diagram of iterative method.

Then we construct $\mathbf{u}^{(n+1)}(\mathbf{x},0)$ from $\mathbf{u}^{(n)}(\mathbf{x},0)$ as follows:

Step.1 Time integrate the linearized Navier-Stokes equation (2) forward with incompressibility $\nabla \cdot \mathbf{u} = 0$ and boundary condition $\mathbf{u} = \mathbf{0}$ from $t = 0$ to $t = T$ with the initial condition $\mathbf{u}^{(n)}(\mathbf{x},0)$ to find $\mathbf{u}^{(n)}(\mathbf{x},T)$.

Step.2 Calculate $\boldsymbol{\nu}^{(n)}(\mathbf{x},T)$ using (22) which is then used as the *initial* condition for the dual linearized Navier-Stokes equation (24).

Step.3 Backwards time integrate the dual linearized Navier-Stokes equation (24) with incompressibility (14) and boundary condition (13) from $t = T$ to $t = 0$ with the 'initial' condition $\boldsymbol{\nu}^{(n)}(\mathbf{x},T)$ to find $\boldsymbol{\nu}^{(n)}(\mathbf{x},0)$.

Step.4 Using equation (23), a simple approach to calculating the correction of $\mathbf{u}^{(n)}$ is as follows:

$$\mathbf{u}^{(n+1)} = \mathbf{u}^{(n)} + \epsilon \left[\frac{\delta G}{\delta \mathbf{u}(\mathbf{x},0)}\right]^{(n)} \tag{26}$$

$$= \mathbf{u}^{(n)} + \epsilon \left(\lambda \mathbf{u}^{(n)}(\mathbf{x},0) - \boldsymbol{\nu}^{(n)}(\mathbf{x},0)\right), \tag{27}$$

with λ chosen such that

$$1 = \left\langle \frac{1}{2}\left\{\mathbf{u}^{(n+1)}(\mathbf{x},0)\right\}^2 \right\rangle \tag{28}$$

$$= \left\langle \frac{1}{2}\left[(1+\epsilon\lambda)\mathbf{u}^{(n)}(\mathbf{x},0) - \epsilon\boldsymbol{\nu}^{(n)}(\mathbf{x},0)\right]^2 \right\rangle. \tag{29}$$

Here ϵ is a parameter of this iterative method and must be sufficiently small.

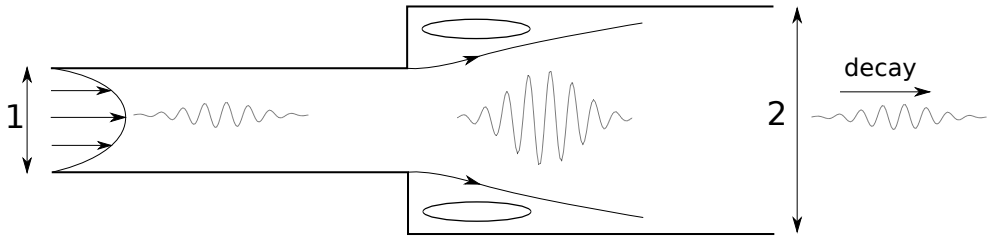

Figure 2: Initial noise is magnified as it passes through the pipe expansion before eventually decaying.

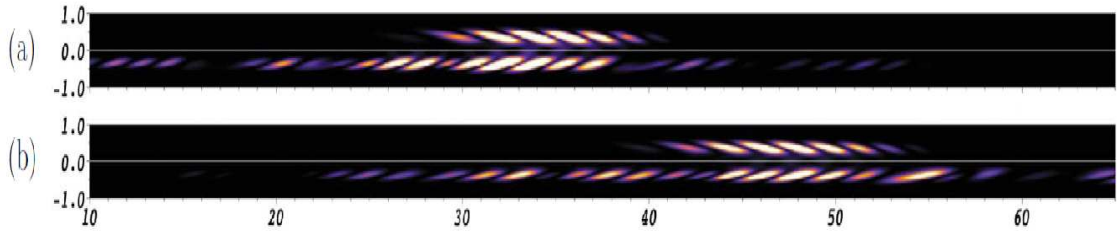

Figure 3: Comparison between noise-driven flows (bottom halves) and the linear optimal growth (top halves) for $Re = 900$ (upper) and $Re = 1200$ (lower) [1].

This last step moves $\mathbf{u}^{(n)}(\mathbf{x}, 0)$ in the direction of maximum ascent in order to increase $G(T)$. Iterating the last four steps typically converges to a local maximum of $G(T)$ [3], [5].

An example of the application of this method for finding linear optimum initial conditions is the case of expansion flow in a pipe [1], see Figure 2. Flow through an expansion in a pipe is a classical engineering problem which is not spatially homogeneous. The resulting linear-growth optimal can be compared with the numerical result of perturbing the flow with random noise, see Figure 3. The dominant spatial structure which grows out of the noise appears to agree well with the linear optimal.

3 Non-linear optimization

The matrix-free approach is, in principle, 'easily' extended to the non-linear problem. There are only two changes that need to be made to the Lagrangian G: the nonlinearity is added back to the linearised Navier-Stokes equation and the initial energy is explicitly set at E_0 which joins T as a free parameter of the problem. So

$$G(T, E_0; Re) = ... + \int_0^T \langle \boldsymbol{\nu} \cdot (\mathbf{u} \cdot \nabla)\mathbf{u} \rangle \, dt + \lambda \left\{ \left\langle \frac{1}{2}\mathbf{u}^2(x, 0) \right\rangle - E_0 \right\} \tag{30}$$

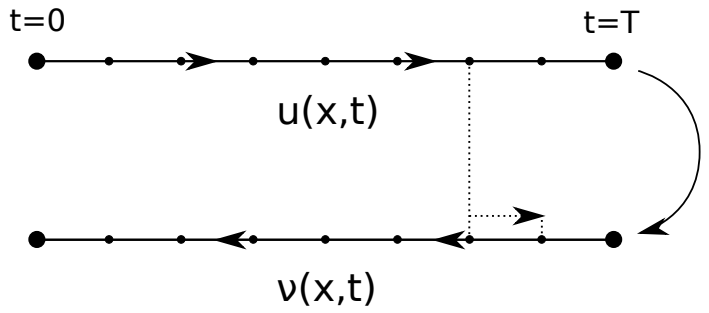

Figure 4: Checkpointing: during the calculation of $\boldsymbol{\nu}(\mathbf{x},t)$ the velocity $\mathbf{u}(\mathbf{x},t)$ is recalculated in short sections from each checkpoint.

The change to a the non-linear term means that the part of the functional derivative of G with respect to $\mathbf{u}$ must be recalculated to get

$$\begin{aligned}\int_0^T \left\langle \frac{\delta G}{\delta \mathbf{u}} \cdot \delta \mathbf{u} \right\rangle dt &= \ldots + \int_0^T \langle \boldsymbol{\nu} \cdot [\delta \mathbf{u} \cdot \nabla \mathbf{u} + \mathbf{u} \cdot \nabla \delta \mathbf{u}] \rangle \, dt \\ &= \ldots + \int_0^T \left\langle \delta \mathbf{u} \cdot [(\nabla \mathbf{u})^{\mathrm{T}} \cdot \boldsymbol{\nu} - \mathbf{u} \cdot \nabla \boldsymbol{\nu}] \right\rangle dt. \end{aligned} \tag{31}$$

Thus the dual Navier-Stokes equation becomes

$$-\frac{\partial \boldsymbol{\nu}}{\partial t} + (\nabla [\mathbf{u} + \mathbf{u}_{lam}])^{\mathrm{T}} \cdot \boldsymbol{\nu} - (\mathbf{u} + \mathbf{u}_{lam}) \cdot \nabla \boldsymbol{\nu} - \nabla \pi - \frac{1}{Re} \nabla^2 \boldsymbol{\nu} = 0. \tag{32}$$

The consequences of adding the non-linear term can be summarised as follows:

1. The full Navier-Stokes equations now need to be integrated forward in time.
2. The dual Navier-Stokes equation remains linear in $\boldsymbol{\nu}$ but now depends on $\mathbf{u}(\mathbf{x},t)$.
3. The result now depends on *both* E_0 and T.

The added dependence of the dual equations on $\mathbf{u}(\mathbf{x},t)$ creates some problems numerically as this suggests that $\mathbf{u}(\mathbf{x},t)$ must be stored at every step of the forwards integration. For large systems the memory requirements associated with this are unfeasible so a method called 'checkpointing' is used instead. This involves storing $\mathbf{u}(\mathbf{x},t)$ at a reduced set of times or 'checkpoints' and then integrating forward in time again from each checkpoint as required when calculating $\boldsymbol{\nu}$, see Figure 4. This method results in much reduced storage requirements but at the added cost of having to perform the forward integration twice per iteration.

4 Results

Before looking at some actual numerical results, we briefly consider what might happen. For a fixed value of T we could expect the algorithm to converge for energy values E_0 where it is not possible to trigger turbulence. However, once E_0 exceeds a threshold E_{thresh} where

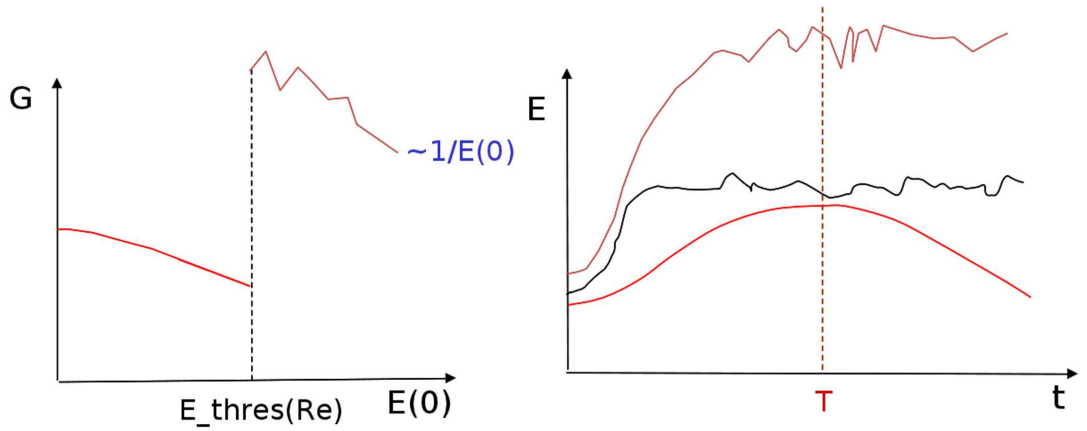

(a) Expected variation of G with E_0.

(b) Possible variations of E with t: turbulent (top), non-linear optimal (middle), linear optimal (bottom).

Figure 5: Expected results; the red curves correspond to the results of linear transient-growth analysis [12].

turbulence can be reached by some initial conditions, the algorithm should find these since they experience the larger energy growth. Then the algorithm should fail to converge due to the extreme sensitivity of the turbulence-triggering initial conditions to the exact turbulent energy level reached a fixed time later: see Figure 5.

4.1 Pipe flow

Pringle & Kerswell [8] numerically solved the nonlinear optimisation problem in the case of pipe flow using a short pipe with $L = \pi R$ (see also [2] for a boundary layer calculation). Figure 6 shows the growth G against E_0 at $Re = 1750$ which indicates how a new 3-dimensional optimal emerges at $E_0 \approx 10^{-5}$ to replace the 2-dimensional linear optimal. The optimisation time T was taken to be the time taken for the linear calculation to reach its maximum value of G to emphasize the effect of nonlinearity in the optimisation calculation. This, however, was too short a time for initial conditions to reach the turbulent state and convergence problems were encountered at $E_0 = 2 \times 10^{-5} < E_{thres}$ (similar issues were also found at $Re = 2250$).

The linear optimal is a well-known 2D structure as shown in Figure 7 (e.g. [12]). The optimum initial disturbance consists of a roll structure which then generates large velocity streaks before eventually decaying back to laminar flow. The structure of the new 3D optimal is much more complicated: see Figure 8. It initially consists of a radially-localised helical mode which unwinds to create rolls which then form streamwise streaks; the presence of these two distinct stages can be clearly seen from the two stages of growth in Figure 6b (see [9] for more details). When similar calculations are performed for longer pipes a localisation of the initial condition in the axial direction is also observed. This localised initial perturbation now also unrolls and expands in the streamwise direction to produce long streamwise rolls and ultimately streaks.

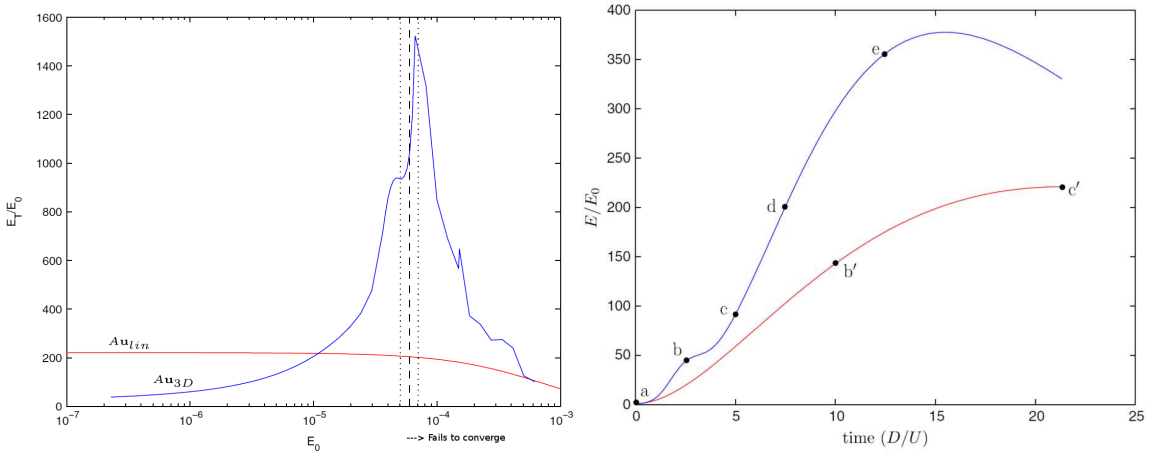

(a) Variation of G with E_0.

(b) Evolution of $G(t)$ with time for linear optimal (lower/red) and non-linear optimal (upper/blue).

Figure 6: Results of numerical calculation for short pipe [8].

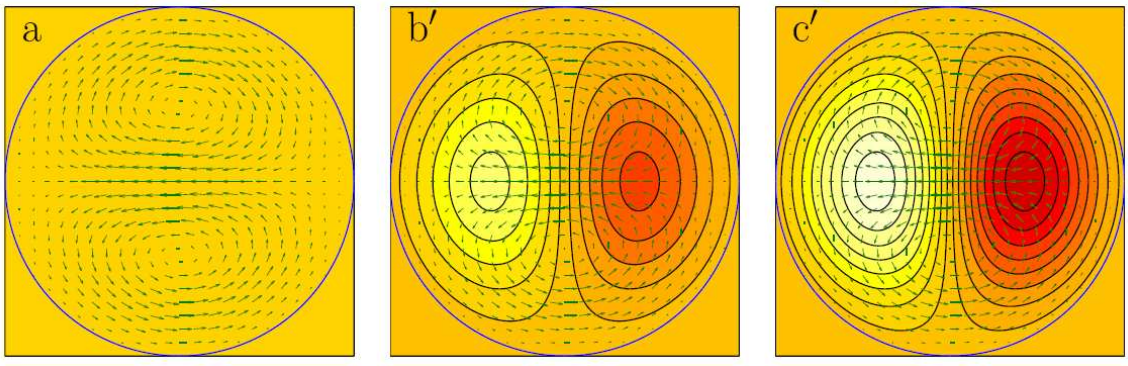

Figure 7: Linear optimal at three successive times. Colours represent streamwise velocity and the arrows represent velocity in the cross-section.

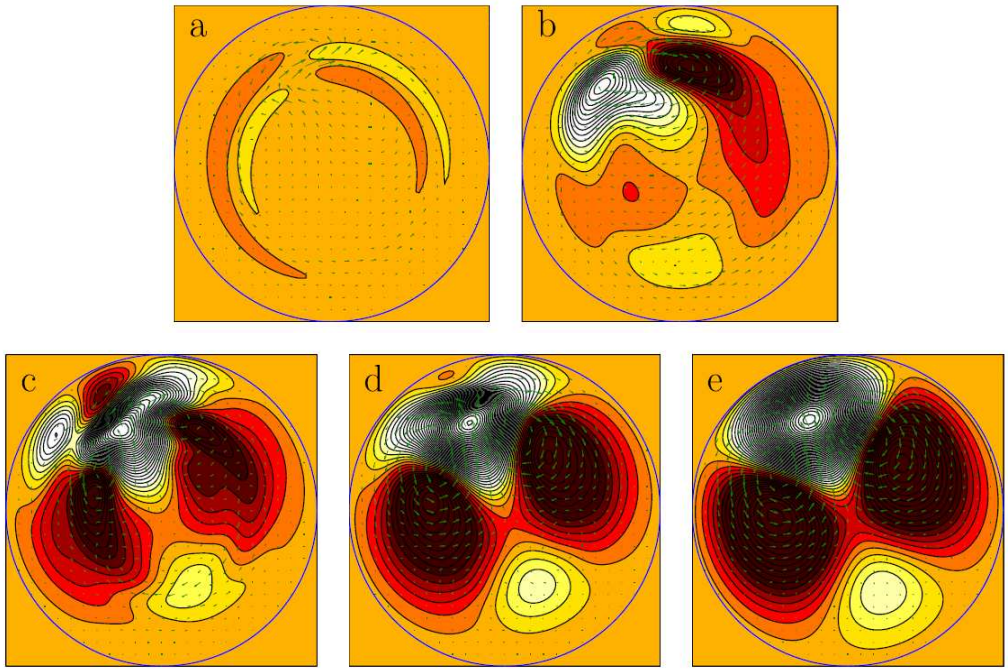

Figure 8: Non-linear optimal at five successive times. Colours represent streamwise velocity and the arrows represent velocity in the cross-section [8].

Two questions emerge from these preliminary results:

1. Can this approach be used to estimate E_{thresh}?
2. Does the non-linear optimal found correspond to the minimal seed for turbulence?

It is clearly possible that the extremum to which the numerical code converges may be a local maximum rather than the global maximum. This would result in too high a value of E_{thresh}. Even if the numerical code finds the correct value of E_{thresh}, it is possible that the non-linear optimum found does not become turbulent but rather the minimal seed is a different point on the same surface of E_0, see Figure 9. Further numerical results [9], however, suggest that the answer to the first question is 'yes' and the answer may also be 'yes' to the second as well.

4.2 PCF

Numerical optimisation calculations have also been performed for PCF [6]. However this work used a different choice of G choosing instead to look at the total dissipation

$$G' = \frac{1}{T}\int_0^T \left\langle \frac{1}{Re}|\nabla \mathbf{u}|^2 \right\rangle dt. \tag{33}$$

This functional was chosen based on the idea that turbulent flow is much more dissipative than laminar flow. The results of these calculations are shown in Figures 10 & 11. The

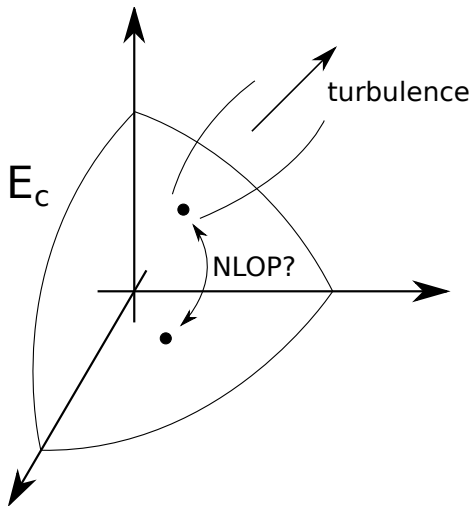

Figure 9: Does the non-linear optimal found numerical necessarily correspond to the minimal seed?

increase in dissipation as the initial condition switches from remaining laminar to transitioning to turbulence is very clear. We also see a localisation of the initial perturbation as was previously observed for a long pipe. Optimising the energy growth for exactly the same flow configuration (geometry and Re) seems to produce the same estimate of E_{thres} [10]. This is consistent with the thinking developed in [9] where the exact functional used is not important but merely that the functional takes on enhanced values for turbulent flow states compared to their laminar counterparts. It should be clear that there is much to explore and understand in this promising new variational approach.

References

[1] C. D. Cantwell, D. Barkley, and H. M. Blackburn, *Transient growth analysis of flow through a sudden expansion in a circular pipe*, Physics of Fluids, 22 (2010), p. 034101.

[2] S. Cherubini, P. De Palma, J.-C. Robinet, and A. Bottaro, *Rapid path to transition via nonlinear localized optimal perturbations in a boundary layer flow*, Phys. Rev. E, 82 (2010), p. 066302.

[3] P. Corbett and A. Bottaro, *Optimal perturbations for boundary layers subject to stream-wise pressure gradient*, Physics of Fluids, 12 (2000), pp. 120–130.

[4] Y. Duguet, L. Brandt, and B. R. J. Larsson, *Towards minimal perturbations in transitional plane couette flow*, Phys. Rev. E, 82 (2010), p. 026316.

[5] A. Guégan, P. J. Schmid, and P. Huerre, *Optimal energy growth and optimal control in swept hiemenz flow*, Journal of Fluid Mechanics, 566 (2006), pp. 11–45.

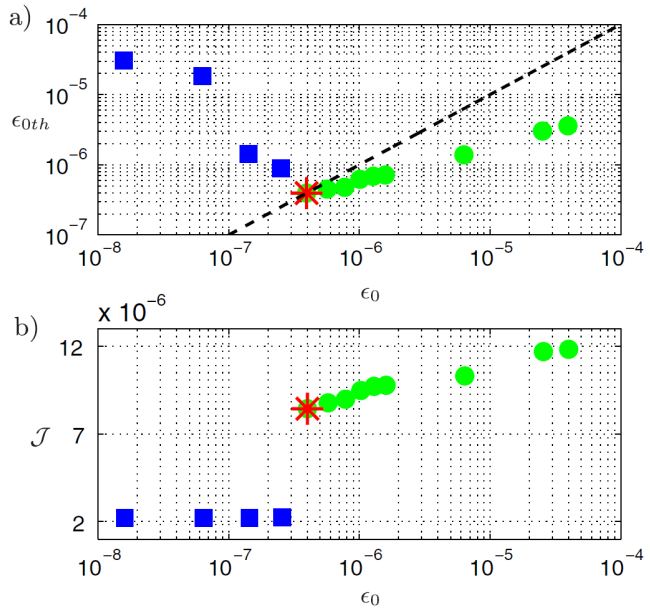

Figure 10: Variation of energy threshold for transition to turbulence with E_0 (top) and of dissipation with E_0 (bottom). Blue marks correspond to flows that remain laminar, green to those that transition to turbulence, and the red star to the non-linear optimal [6].

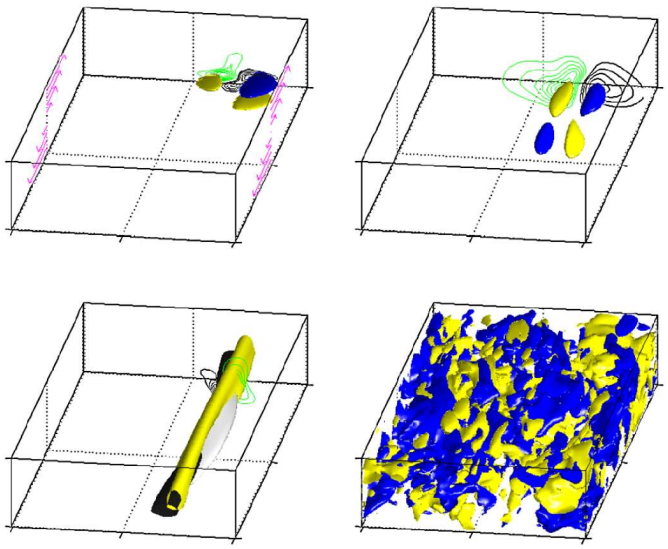

Figure 11: Evolution of the non-linear optimal with time [6].

[6] A. Monokrousos, A. Bottaro, L. Brandt, A. Di Vita, and D. S. Henningson, *Nonequilibrium thermodynamics and the optimal path to turbulence in shear flows*, Phys. Rev. Lett., 106 (2011), p. 134502.

[7] C. C. T. Pringle and R. R. Kerswell, *Asymmetric, helical and mirror-symmetric travelling waves in pipe flow*, Phys. Rev. Lett., 99 (2007), p. 074502.

[8] ——, *Using nonlinear transient growth to construct the minimal seed for shear flow turbulence*, Phys. Rev. Lett., 105 (2010), p. 154502.

[9] C. C. T. Pringle, A. P. Willis, and R. R. Kerswell, *Minimal seeds for shear flow turbulence: using nonlinear transient growth to touch the edge of chaos*, arXiv:1109.2459v1, (2011).

[10] S. M. E. Rabin, C. P. Caulfield, and R. R. Kerswell, *Variational identification of minimal seeds to trigger transition in plane Couette flow*, arXiv:1111.6654, (2011).

[11] S. C. Reddy and D. S. Henningson, *Energy growth in viscous channel flows*, Journal of Fluid Mechanics, 252 (1993), pp. 209–238.

[12] P. J. Schmid and D. S. Henningson, *Optimal energy density growth in hagen-poiseuille flow*, Journal of Fluid Mechanics, 277 (1994), pp. 197–225.

[13] D. Viswanath and P. Cvitanović, *Stable manifolds and the transition to turbulence in pipe flow*, Journal of Fluid Mechanics, 627 (2009), pp. 215–233.